Performance Characterization of Spatially Random Energy Harvesting Underlay D2D Networks with Transmit Power Control

S. Kusaladharma and C. Tellambura, *Fellow*, *IEEE*

Department of Electrical and Computer Engineering

University of Alberta, Edmonton, Alberta T6G 2V4, Canada

Email: kusaladh@ualberta.ca and chintha@ece.ualberta.ca

Abstract

In underlay device-to-device (D2D) networks, the transmitter nodes can harvest energy from downlink cellular (primary) transmissions to solely power the D2D links, which enhances the overall spectral and energy efficiencies. How will the energy harvest and D2D link performance be affected by spatial randomness, temporal correlations, transmit power control, and channel uncertainties? To investigate these issues, we analyze the energy harvesting process of a random (typical) D2D transmitter node, say $\mathcal{D}_t$, which needs a sufficient harvest to meet the requirements for receiver sensitivity and channel inversion. This system model consists of (a) three independent homogeneous Poisson point processes, (b) log-distance path loss and Rayleigh fading, and (c) path loss inversion (PLI) transmit power control. We derive the ambient radio frequency (RF) energy at $\mathcal{D}_t$, and model the harvest as a Gamma random variable. We propose four schemes: single slot harvesting, multi slot harvesting, $\mathcal{N}$ slot harvesting, and hybrid harvesting. We develop a Markov chain model for success probability of these schemes, and derive the D2D coverage. We find that a high density of primary transmitters is unfavorable to multi slot harvesting for increased D2D link distances. Moreover, hybrid harvesting always outperforms single and $\mathcal{N}$ slot harvesting, and outperforms multi-slot harvesting except for very high path-loss conditions.

Index Terms

Energy harvesting, D2D networks, Stochastic geometry, Aggregate interference

This paper was presented in part at the IEEE International Communications Conference (ICC), Paris, France, 2017 [1]. It has received the best paper award from the Green Communications Systems and Networks Symposium.

I. INTRODUCTION

D2D networks are a special case of underlay cognitive radio (CR) paradigm, which allows simultaneous spectrum access for primary and secondary users in an interference tolerant basis [2], [3]. Moreover, D2D can underlay the existing cellular networks, and in multi-channel cognitive cellular networks, where macro base stations (BSs) are underlaid with cognitive femtocell BS. The essential D2D concept is to allow proximate nodes to mutually communicate without using the resources of the base station [4], which alleviates the spectral efficiency constraints that hamper the continued growth of wireless systems [5], [6]. Thus, D2D allows traffic offloading between users, improves utilization of spectral resources, increases capacity, and lowers the delay [7], [8]. However, to manage the D2D interference on primary network, exclusion regions and transmit power constraints are imposed on the D2D nodes, which will hinder the throughput of the D2D network.

In principle, D2D nodes can harvest energy and spend the harvest to power their transmissions. However, the uncertainty of energy harvests and interference from other co-channel transmissions are significant challenges. Nevertheless, radio frequency (RF) energy harvesting has received heightened attention [9], which allows D2D nodes to improve their energy efficiency [10]–[14]. Although current harvesting circuits have limited capability, D2D nodes need only low power because they have to limit their interference on the primary network. Thus, energy harvesting might be just enough. However, spatial randomness of radio nodes, transmit power control and propagation effects make the harvest stochastic [15], [16]. Thus, the power levels and frequency of transmissions of D2D nodes may not be viable at times. Overall, proper design of energy harvesting schemes is vital to ensure reasonable performance.

A. Motivation and Contributions

In this paper, we investigate the energy harvesting process of a typical underlaid D2D node, $\mathcal{D}_t$, from the down-link transmissions of a multi-channel primary cellular network. The amount of energy harvested, say, E_h depends on the distances from $\mathcal{D}_t$ to the set of primary base-stations, transmit power control and channel conditions. Having collected energy E_h, which is random, $\mathcal{D}_t$ is ready to communicate with its associated D2D receiver. Note that E_h may not be sufficient if the path loss is large due to the receiver distance and if the received power in the D2D link falls below the sensitivity threshold. In order to reduce this risk, we can consider energy harvests spanning multiple harvesting periods. Thus, suitable harvesting schemes are needed to

ensure regular data transmission and sufficient energy harvests. Moreover, path loss inversion (PLI) transmit power control employed by both cellular and D2D transmitters will affect both aggregate interference and link performance.

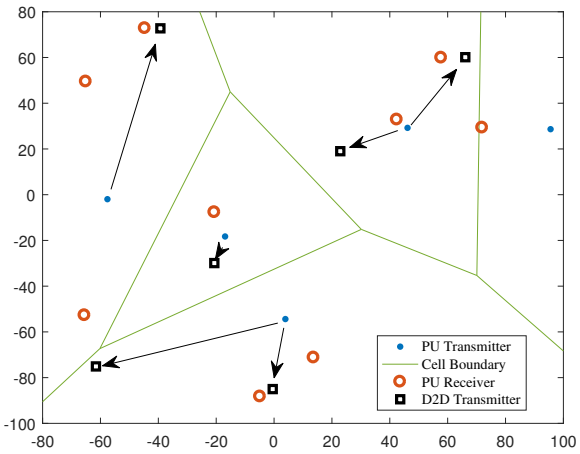

Fig. 1: System model.

The specific problem investigated in this paper can be explained as follows. In Fig. 1, D2D nodes and cellular nodes (e.g., user equipment and base stations) share the same spectrum, and D2D nodes harvest the RF energy from cellular downlink transmissions. Each cell has K downlink channels and all base-stations are synchronous at network level. Our goal is to analyze the cumulative effects of all spatial, channel, and power control effects on the amount of energy extracted by a typical D2D node ($\mathcal{D}_t$) and to develop suitable harvesting schemes. While the interference on primary cellular users from D2D transmissions is also a critical concern, we will leave this for a future work. To study the impact of spatial randomness in $\mathbb{R}^2$, we model primary transmitters, primary receivers and D2D transmitters as three independent homogeneous Poisson point processes (PPPs) (Fig. 1) , where primary receivers associate with their closest primary transmitters and each D2D transmitter is associated with a corresponding receiver randomly distributed within a given distance from it. To model propagation effects, log distance path loss and Rayleigh fading are assumed. The primary spectrum is divided into multiple sub-bands. All transmitters use path-loss inversion based power control. Furthermore, an exclusion region prohibiting D2D transmissions is enforced around every primary receiver. The D2D transmitters harvest ambient RF energy from the primary system and transmit their data within a single sub-band. Our contributions can be summarized as follows:

1) The aggregate ambient RF power at a typical $\mathcal{D}_t$ is the critical quantity. By using stochastic geometry, we derive its moment generating function (MGF), mean and variance, and model it as a Gamma random variable using moment matching. The derivation of the MGF is complicated by the fact that K sub-bands are used by each base station, and because separated power control schemes are employed for each sub-band by every base station. As an auxiliary result, we also derive the probability of a primary transmitter using a particular sub-band when cellular users are assigned any of the K sub-bands randomly without any specific priority.
2) We propose four energy harvesting protocols for a typical D2D transmitter node $\mathcal{D}_t$:
    a) Single time-slot harvest - $\mathcal{D}_t$ harvests for one period and then transmits irrespective of the harvested energy.
    b) Multi slot harvest - $\mathcal{D}_t$ continues till the harvested energy satisfies transmission requirements.
    c) $\mathcal{N}$ slot harvesting scheme - $\mathcal{D}_t$ harvests for $\mathcal{N}$ slots before it transmits.
    d) Hybrid harvesting - $\mathcal{D}_t$ can harvest energy for a maximum of $\mathcal{N}$ slots, and the harvesting process stops whenever extracted energy satisfies the transmission requirements.

    The detailed descriptions of these can be found Section II.D.
3) We derive the probability of a successful energy harvest and being ready to transmit for the four aforementioned schemes. Because temporal dynamics are at play, we utilize Markov chains to model state transitions. Furthermore, we analyze the steady state probability of being within the desired states.
4) We characterize the D2D link coverage performance for a channel assignment protocol where each D2D transmitter selects a random sub-band for its transmission, for the four proposed energy harvesting schemes. In deriving this, we consider the interference from other D2D nodes and the cellular transmissions using the same sub-band.

B. Related Work

Energy-harvesting D2D nodes within a cellular setup has received significant interest recently [4], [8], [17]–[21]. Reference [4] is the closest to the present work, and it investigates the feasibility of energy harvesting by D2D nodes within a multi-channel cellular system using stochastic geometry. This work assesses prioritized and random spectrum access policies for the D2D network, where the communication procedure is successful if both the energy harvesting

process and the subsequent transmission are successful. It is found out that the D2D nodes are able to harvest sufficient energy to allow for their own transmissions, and that prioritized spectrum access provides better performance. However, a key difference from our work is that [4] does not consider power control procedures, which will significantly alter the ambient RF power. Moreover, while [4] focuses more on sub-channel assignment policies, our work will analyze different energy harvesting protocols.

On the other hand, while the works [17]–[19] incorporate temporal correlations in their analysis based on Markov chains, they do not investigate different energy harvesting protocols, a multi channel set-up, and power control. The work in [18] was pioneering in using Markov chains and stochastic geometry to analyze the performance of an energy harvesting network. The authors consider a set of random primary and secondary nodes which communicate with their receivers located a fixed distance away, and derives the optimal transmit power and secondary user density to achieve maximum throughput. Moreover, [17] analyzes the network performance when user-equipment relays harvest energy, and the authors develop an analytical framework and model the status of the harvested energy, while [19] introduces a tractable K-tier heterogeneous model with energy harvesting base stations.

The works [8], [20], [21] consider random networks based on the Poisson point process model. The fundamental trade-offs between the number of D2D transmissions and the harvesting period, and the optimum spectrum partitioning factor are characterized [8]. Similarly, [20] investigates the effects of allowing multiple-hop transmissions when the harvested energy is insufficient, finding that two hop outperforms single hop communication. Going a step further, [21] incorporates massive MIMO (Multiple input multiple output) nodes in characterizing the efficiency of energy harvesting D2D networks.

While other works also consider energy harvesting based networks, they do not consider either power control, a multi-channel cellular setup, temporal correlations, or spatial randomness via the Poisson model. However, a common theme in most of these works is the characterization of ambient signal power at a D2D harvesting device. For example, a novel energy field model is introduced in [22] and the coverage probability of a cellular network powered by energy harvesting is characterized. In addition, [23] proposes dynamic spectrum and power allocation schemes, while [24] investigates the resource management problem of energy harvesting for an uplink cellular set-up

Notations: $\Gamma(x,a) = \int_a^\infty t^{x-1}e^{-t}dt$ and $\Gamma(x) = \Gamma(x,0)$. $\Pr[A]$ is the probability of event A,

Name	PDF
λ_{pt}	Primary transmitter density
λ_{pr}	Primary receiver density
Φ_{d2d}	PPP of D2D transmitters
λ_{d2d}	D2D transmitter density
d_l	Maximum D2d transmitter-receiver distance
$\rho_*, * \in \{p, d2d\}$	Receiver sensitivity of primary and D2D receivers
d_g	Guard distance
$\mathcal{A}_\mathcal{G}$	Area of all the guard regions
ν	Probability of a D2D transmitter being outside $\mathcal{A}_\mathcal{G}$
α	Path loss exponent
β	Energy harvesting efficiency
$\mathcal{N}$	Number of time slots for $\mathcal{N}$ slot and hybrid schemes
K	Number of frequency sub-bands used by the primary system
P	Received ambient RF power
$C_{k,l}$	Probability that the k-th sub-band is in operation of the l-th primary transmitter
τ	Probability that the D2D transmitter fails to harvest the required transmission energy within the energy harvesting period
$p*, * \in \{ss, ms, \mathcal{N}, hs\}$	Probability of a D2D transmitter being able to transmit at the start of a time slot given that it is outside $\mathcal{A}_\mathcal{G}$
γ_T	SINR reception threshold
σ_n^2	Noise power spectral density
I_p	Interference from primary transmissions
I_{d2d}	Interference from D2D transmissions
$\mathbb{P}_C$	Coverage probability given a transmission occurs
$\mathbb{P}_{C,Total}$	Coverage probability of a successful transmission

TABLE I: List of commonly used symbols.

$f_X(\cdot)$ is the probability density function (PDF), $F_X(\cdot)$ is the cumulative distribution function (CDF), $M_X(\cdot)$ is the MGF, and $\mathbb{E}_X[\cdot]$ denotes the expectation over random variable X.

II. System Model

We next describe the spatial distribution of primary and D2D nodes, the wireless channel model, receiver selection schemes, and power control procedures.

A. Spatial Distribution

The network is broadly divided into primary and D2D nodes, both of which are co-located but separate. Therefore, primary receivers do not switch to be a D2D node and vice-versa.

1) Primary Network Distribution: Primary transmitters (base stations) and primary receivers (users) are randomly distributed in $\mathbb{R}^2$. Base station locations have traditionally been pre-planned, giving rise to the hexagonal grid structures centered on base stations. However, with the advent of heterogeneous femto, pico and macro cells, such regular grids have been replaced with irregular and random structures. Therefore, the resulting spatial randomness must be captured by a suitable spatial point process. By far, the Poisson point process has been the most popular one [25]–[28], which not only has analytical tractability, but also has the ability to accurately approximate planned network set-ups [29].

We will thus model primary nodes and D2D transmitters as homogeneous Poisson point processes, where the intensity of the process (average node density) is constant everywhere. While non-homogeneous processes perhaps suit actual real-world scenarios better, they are not amenable to more general analysis. A characteristic property of a homogeneous Poisson point process is that the number of nodes $N(\mathcal{A})$ within an enclosed area $\mathcal{A} \subset \mathbb{R}^2$ is Poisson distributed with [30], [31]

$$\Pr[N(\mathcal{A}) = n] = \frac{(\lambda \mathcal{A})^n}{n!} e^{-\lambda \mathcal{A}}, \quad n = 0, 1, \ldots \tag{1}$$

where $\lambda > 0$ is the average number of nodes per unit area. Accordingly, we model the primary transmitters (e.g., base stations) and receivers with two such processes Φ_{pt} and Φ_{pr} with intensities $\lambda_{pt}(> 0)$ and $\lambda_{pr}(> 0)$. Furthermore, since a base station typically serves multiple receivers, we further assume that $\lambda_{pt} < \lambda_{pr}$. Moreover, it is assumed that Φ_{pt} and Φ_{pr} are stationary, and mutually independent. All these assumptions are standard in the literature.

The primary network employs universal frequency reuse [4], [32]. The frequency band which is used for the downlink is divided into $K > 1$ sub-channels where each can accommodate a different primary receiver [4]. In practical terms, these sub-channels are resource blocks associated with modern cellular networks such as LTE (Long Term Evolution) systems [33].

2) D2D Network: This consists of transmitter and receiver pairs, and are distributed in $\mathbb{R}^2$. We model the D2D transmitters as homogeneous Poisson point process Φ_{d2d} with intensity $\lambda_{d2d}(> 0)$. On the other hand, the D2D receivers are distributed uniformly in an annular area of radius d_l centered on each D2D transmitter. Without loss of generality, each D2D transmitter

is associated with a unique receiver with a probability of one. However, if this probability is less than one, say, κ, then Colouring Theorem [30] shows that the associated D2D transmitters follow a thinned homogeneous Poisson process whose intensity is $\hat{\lambda}_{d2d} = \kappa\lambda_{d2d}$[1].

B. Channel Model

As is customary, the propagation model incorporates power-law path loss and small scale fading. We assume the simplified path loss model [34] where the received power P_R at a distance r from the transmitter of power P_T is $P_R = P_T r^{-\alpha}$, where α is the path loss exponent ranging from 2 to 6 [35]. The value of α is assumed to be constant within the k sub-bands. However, this model does not hold whenever $r \to 0$ as the received power $P_R \to \infty$. This difficulty is avoided via $P_R = P_T \left(\max(\delta, r)\right)^{-\alpha}$ where $\delta = 1$ is the reference distance. Because the probability of event $\{r \leq \delta\}$ is very small, this alteration does not significantly affect the overall statistics [36].

The small-scale fading follows the Rayleigh fading model. Consequently, the channel power gain $|h|^2$ is exponentially distributed with $f_{|h|^2}(x) = e^{-x}, \quad 0 < x < \infty$. The fading gains of different links are mutually independent. These assumptions are standard in the literature. However, it should be noted that in practice, there is correlation between the fading of nearby links. An investigation on the effects of correlation is beyond the scope f this paper.

C. Power Control and Transmitter-receiver Association

All transmitters employ PLI power control scheme in order to ensure a fixed received power level on average, which is the minimum signal power required to produce a specified performance of the receiver. The level is called the receiver sensitivity[2]. Clearly, the receiver sensitivity and distance determine the transmit power requirement. For example, let the primary and D2D receivers have sensitivities ρ_p and ρ_{d2d}, and the receiver distance be r, then the transmit power can be written as $P_T = \rho_* r^{\alpha}$, where ρ_* is the receiver sensitivity depending on the network [37]. Although this can potentially lead to excessive transmit powers, this difficulty is alleviated in our system model due to two reasons. First, primary transmitters are grid-connected base stations and are not peak-power constrained. Second, D2D transmitter-to-receiver distance is less than the

[1]Here is an equivalent alternative interpretation. The D2D transmitters and receivers form separate independent Poisson point processes, and each transmitter randomly selects a receiver within a distance d_l, where a receiver can be connected to multiple transmitters concurrently.

[2]The instantaneous received power vary with small scale fading

radius d_l, which naturally limits the peak-power requirement, which is $\rho_{d2d} d_l^{\alpha}$. While improving the power control scheme is possible by considering channel gains, receiver interference levels, and different transmission thresholds, we defer this for future work.

The primary transmitter and receiver nodes are paired according to the closest association rule [36]. Thus, the link distance is minimized, and this pairing is implemented with the help of GPS (Global Positioning System) information, location databases, or periodic fixed-power pilot sequences [38]. In general, the closest receiver link provides the best received power on average. This association policy divides the coverage area into Voronoii cells surrounding each primary transmitter. In each such cell, all primary receivers associate with the primary transmitter. We assume that there are no out-of-cell associations. Accordingly, the primary receiver-to-transmitter distance relates to the void probability of a Poisson point process, and follows the Rayleigh distribution with [30]

$$f_X(x) = 2\pi\lambda_{pt} x e^{-\pi\lambda_{pt} x^2}, 0 < x < \infty. \tag{2}$$

Without any loss of generality, we assume that all primary receivers connect with a primary transmitter, and that no receiver is idle unless all the sub-bands of the transmitter are occupied. The Colouring theorem [30] can be easily employed if only a subset of the primary receivers need to be serviced at any given time.

For the D2D network, however, the transmitter-receiver distance is obtained as follows. With respect to any transmitter, the receiver can be uniformly located within an annular region of radius d_l [4]. Thus, the CDF of the transmitter-receiver distance is $F_X(x) = \frac{\pi x^2}{\pi d_l^2}$, $0 < x < d_l$. Differentiating this CDF yields the linear PDF

$$f_X(x) = \frac{2x}{d_l^2}, 0 < x < d_l. \tag{3}$$

Just like the primary transmitters, without loss of generality, each D2D transmitter is ready to transmit at any time instant.

As mentioned before, to limit D2D interference on the primary network, guard regions must be employed [39]. These are D2D-free zones around the primary users, and clearly limit the potential interference. Their existence can be broadcast dynamically through periodic control sequences from the primary users [36], [40]. There are two placement options for the guard zones: (1) around primary receivers or (2) around primary transmitters. We assume the former, but not the latter. This assumption is selected due to several reasons. First, what is needed

to be ensured in the underlay mode is the interference temperature at each primary receiver being below a threshold. Thus, placement of guard zones around primary receivers make sense. Second, if option two is adopted, the primary receivers outside or close to the cell edge may not be detected by the sensing algorithm and will suffer interference. Third, as energy must be harvested from primary transmissions, the close proximity of D2D nodes to primary transmitters reduces the path loss and increases the energy harvest , but option two prevents that.

The guard regions are assumed to be annular regions with a radius of d_g for mathematical tractability. It should be noted that shadowing introduced by terrain conditions such as buildings hills can make an annular region non-optimal. Let Φ_{pr} be denoted by the set of points $\{x_1, x_2, ...\}$, and $\phi_{pr,i}$ be the primary receiver located at $x_i, (x_i \in \Phi_{pr})$. The guard region encircling $\phi_{pr,i}$ is thus denoted as $b(x_i, d_g)$. Therefore, if Φ_{d2d} is represented by $\{y_1, y_2, ...\}$, and node $\mathcal{D}_t$ is a typical D2D transmitter located at y_j ($j \in \Phi_{d2d}$), it is precluded from transmitting if $y_j \in \mathcal{A}_{\mathcal{G}}$. Here, $\mathcal{A}_{\mathcal{G}} \in \mathbb{R}^2$ is the area of all the guard regions given by $\mathcal{A}_{\mathcal{G}} = \bigcup_{i \in \Phi_{pr}} b(x_i, d_g)$. Now, let the process of D2D transmitters outside $\mathcal{A}_{\mathcal{G}}$ be denoted as $\tilde{\Phi}_{d2d}$. $\tilde{\Phi}_{d2d}$ is non-homogeneous, and forms what is termed a Poisson hole process [39]. Let ν be the probability that node $\mathcal{D}_t$ lies outside $\mathcal{A}_{\mathcal{G}}$, and alternatively is the probability that no primary receiver falls within a distance d_g from node $\mathcal{D}_t$. We can thus obtain ν from (1) as $\nu = e^{-\pi \lambda_{pr} d_g^2}$.

D. D2D Network Operation

The D2D transmitters are solely powered by the energy harvested from ambient primary RF emissions. We assume that the power conversion circuits have an efficiency of $\beta(< 1)$, and that energy is harvested in the downlink phase from all sub-bands. Let a primary downlink time slot have length T. If the D2D transmitter requires additional energy at the beginning of a time slot, it will allocate the entire time slot for energy harvesting. Therefore, even in the best case scenario when the required energy is harvested in each time slot, data transfer is performed only on 50% of the time slots.

Energy harvesting is subject to inherent unreliability because the harvested amount may not be enough to ensure that the receiver sensitivity is met [4]. Moreover, if harvesting time increases, the fraction of time available for data transfer will decrease, increasing delay and reducing spectral efficiency. To balance such conflicting requirements, we next propose four different energy harvesting schemes for a typical D2D transmitter (i.e., node $\mathcal{D}_t$ for brevity). The four schemes are subject to two common conditions. First, $\mathcal{D}_t$ uses up all harvested energy for its own

transmissions and returns to zero power state after each transmission. This assumption leads to a worst case performance as there may be some residual energy remaining in the batteries after a transmission takes place. However, this assumption makes the Markov chain based analysis more tractable as we will see in the next few sections. Second, the transmission of $\mathcal{D}_t$ are subject to the guard zones around primary receivers (i.e., there are no transmissions).

1) Single-slot harvesting

- Energy is harvested in slot 1. Let the power level associated with this energy be P_{EH} (the energy harvesting process is explained in detail in the subsequent sections). $P_{EH} = \beta PT$ where the ambient RF power at node $\mathcal{D}_t$ is P.
- If $P_{EH} < P_{TT}$, node $\mathcal{D}_t$ transmits at P_{EH} during the subsequent time slot as long as it is outside the guard region $\mathcal{A}_{\mathcal{G}}$. Here, P_{TT} is the required transmit power to ensure the receiver's sensitivity with PLI power control given by $P_{TT} = \rho_{d2d} r_{d2d}^{\alpha} T$, where r_{d2d} denotes the distance between node $\mathcal{D}_t \in \Phi_{d2d}$ and its receiver.
- If $P_{EH} > P_{TT}$, node $\mathcal{D}_t$ transmits at P_{TT} during the subsequent time slot.
- If node $\mathcal{D}_t$ is within $\mathcal{A}_{\mathcal{G}}$, no transmission occurs.

Note that although data transmission occurs irrespective of the harvested energy level, the transmit power level could vary. If enough energy is harvested, PLI power control ensures that node $\mathcal{D}_t$ has enough to satisfy the receiver's sensitivity requirement. But, if this is not satisfied, the transmission occurs using the harvested energy without any power control procedure. This scheme is most appropriate when the D2D users must transfer time critical data to because a transmission is guaranteed every two time slots subject to node $\mathcal{D}_t$ being outside a guard region.

2) Multi-slot harvesting

Node $\mathcal{D}_t$ waits multiple time slots till the harvested energy is greater than the required transmission energy to ensure the receiver's sensitivity requirement through PLI power control. The specific protocol is as follows.

- Energy is harvested in slot 1.
- If $P_{EH} < P_{TT_m}$, energy harvesting occurs at the subsequent time slot. This process continues till $P_{EH} > P_{TT_m}$, where P_{TT_m} is the maximum energy required to transmit,

given by $P_{TT_m} = \rho_{d2d} d_l^{\alpha} T$.

- Whenever $P_{EH} > P_{TT_m}$, node $\mathcal{D}_t$ transmits at P_{TT_m} during the subsequent time slot as long as $\mathcal{D}_t$ is outside $\mathcal{A}_{\mathcal{G}}$.
- If node $\mathcal{D}_t$ is within $\mathcal{A}_{\mathcal{G}}$, no transmission occurs.

However, if this sensitivity requirement is high or if the ambient RF energy from the primary system is low, it can take a significant amount of time slots for node $\mathcal{D}_t$ to charge fully, which reduces its ability to transmit at the start of a given time slot. On the flip side, the eventual transmission has a high probability of success to ensure that receiver sensitivity requirements are met. This scheme is most suitable under one or more of the following conditions: the data is not time critical and the data generation is irregular and infrequent.

3) $\mathcal{N}$-slot harvesting

This is an extension of the single slot harvesting scheme to $\mathcal{N}$ slots, and the protocol can be summarized as below.

- Energy is harvested by node $\mathcal{D}_t$ in slots 1 to $\mathcal{N}$.
- If $P_{EH} < P_{TT}$, node $\mathcal{D}_t$ transmits at P_{EH} during the subsequent time slot $(\mathcal{N}+1)$.
- If $P_{EH} > P_{TT}$, node $\mathcal{D}_t$ transmits at P_{TT} during the subsequent time slot.
- If the D2D transmitter is within $\mathcal{A}_{\mathcal{G}}$, no transmission occurs.

While keeping the regularity of single slot harvesting, $\mathcal{N}$ slot harvesting attempts to harvest more energy before the transmission is conducted so that the resulting transmission is successful. Moreover, similar to single slot harvesting, transmission occurs irrespective of the harvested energy after $\mathcal{N}$ harvesting slots. With this scheme, the selection of $\mathcal{N}$ must be performed judiciously. While a small $\mathcal{N}$ provides regular transmission opportunities, it also constrains the harvested power.

4) Hybrid harvesting

Hybrid harvesting is a cross between $\mathcal{N}$ slot harvesting and multi slot harvesting. Within this scheme, node $\mathcal{D}_t$ can harvest energy for a maximum of $\mathcal{N}$ slots. However, if the

harvested energy exceeds P_{TT} before the $\mathcal{N}$ slots are up, node $\mathcal{D}_t$ aborts the harvesting and transmits within the subsequent slot. In other words, the hybrid harvesting scheme is multi slot harvesting with a cap of $\mathcal{N}$ harvesting slots. If the harvested energy is still lower than P_{TT} after $\mathcal{N}$ time slots, node $\mathcal{D}_t$ has no option other than transmitting using the harvested energy as long as it is outside the guard region $\mathcal{A}_{\mathcal{G}}$. This scheme keeps the predictability of the $\mathcal{N}$ slot harvesting scheme by forcing a transmission after a pre-determined period. But it goes a step further by providing the flexibility to cease energy harvesting if the required energy amount is harvested before $\mathcal{N}$ periods. The specific protocol can be summarized as below.

- Energy is harvested in slot 1.
- If $P_{EH} < P_{TT}$, energy harvesting ocurs at the subsequent time slot. This process continues till either $P_{EH} > P_{TT}$ or till the $\mathcal{N}$-th time slot.
- Whenever $P_{EH} > P_{TT}$, node $\mathcal{D}_t$ transmits at P_{TT} during the subsequent time slot as long as it's outside the guard region $\mathcal{A}_{\mathcal{G}}$.
- If $P_{EH} < P_{TT}$ even after the $\mathcal{N}$-th time slot, node $\mathcal{D}_t$ transmits at P_{EH} during the subsequent time slot as it's outside the guard region $\mathcal{A}_{\mathcal{G}}$.
- If the D2D transmitter is within $\mathcal{A}_{\mathcal{G}}$, no transmission occurs.

As mentioned before, the D2D transmitters use one of the $K > 1$ different sub-bands for their transmissions. The selected sub-band determines the resultant interference on both the primary and D2D receivers. To limit this, we will consider the random selection of a sub-band by each D2D transmitter. This protocol reduces lower intra-D2D interference as the different D2D transmissions may occur in different sub-bands. However, on the downside, as no particular band is free from a potential D2D access, all primary transmissions may be adversely effected.

III. Energy Harvesting

In this section, we will derive total harvested energy in each of the four harvesting schemes and the probability of a successful energy harvest within the harvesting period.

In many cases, since exact distributions of random variables are generally intractable, MGF (moment generating function) is widely used [28], [32], [41]–[45]. The MGF can be obtained relatively easily when there is a sum of independent variables [28], [41].

Let P be the received ambient RF power (i.e., βPT is the harvested energy) at node $\mathcal{D}_t$, which we place at the origin without the loss of generality. Ambient power P emanates from all

primary transmitters, hence we write $P = \sum_{l\in\Phi_{pt}} P_l$, where P_l is the ambient RF power from the l-th primary transmitter $\phi_{pt,l}$. P_l is written as $P_l = \sum_{k=1}^{K} C_{k,l}\rho_p \hat{r}_{k,l}^{\alpha}|h_l|^2 g(r_l)$, where the term $\rho_p \hat{r}_{k,l}^{\alpha}$ is the transmit power from $\phi_{pt,l}$ to the primary receiver using the k-th sub-band located at a distance of $\hat{r}_{k,l}$ from it. Quantities $|h_l|^2$ and $g(r_l) = \min(1, r_l^{-\alpha})$ are respectively small-scale channel power gain and the path loss between $\phi_{pt,l}$ and $\mathcal{D}_t$, and $C_{k,l}$ is the probability that the k-th ($1 \leq k \leq K$) sub-band is in occupation during the specific harvesting time-slot.

To conduct further analysis with P, we will evaluate its MGF, which is defined as $M_P(s) = \mathbb{E}[e^{-sP}]$. Using Campbell's Theorem [30], we can write $M_P(s)$ as

$$M_P(s) = e^{\int_0^{\infty} \mathbb{E}\left[e^{-s\sum_{k=1}^{K} C_{k,l}\rho_p \hat{r}_{k,l}^{\alpha}|h_l|^2 g(r_l)}-1\right] 2\pi\lambda_{pt} r_l dr_l}. \tag{4}$$

Using the fact that $\frac{1}{1+x} = \sum_{v=0}^{\infty}(-x)^v$, and averaging with respect to $|h_l|^2$ and r_l we can simplify $M_P(s)$ as [36]

$$M_P(s) = e^{\left(\sum_{v=1}^{\infty} \frac{\pi\lambda_{pt}\alpha v}{\alpha v-2}(-sC_{k,l}\rho_p)^v \mathbb{E}[(\sum_{k=1}^{K} \hat{r}_{k,l}^{\alpha})^v]\right)}. \tag{5}$$

Because P and its MGF are of complicated forms, it is advantageous to approximate P with a well known r.v. It has been shown that the received power from a random field of base stations follows a skewed α-stable distribution, which can be closely modeled as a Gamma r.v. with hape and scale parameters k_P and θ_P respectively [41]. For this, we can match actual moments of P are with those of the Gamma r.v. To this end, we use MGF to derive the moments of P, where the n-th moment is given by $\mathbb{E}[P^n] = (-1)^n \left[\frac{d^n}{ds^n} M_P(s)\right]_{s=0}$. Therefore, we can find $\mathbb{E}[P]$ and $\mathbb{VAR}[P]$ when $\alpha > 2$ as follows:

$$\mathbb{E}[P] = \frac{\Gamma\left(\frac{\alpha}{2}+1\right)\alpha K C_{k,l}\rho_p}{(\pi\lambda_{pt})^{\frac{\alpha}{2}-1}(\alpha-2)}, \tag{6}$$

$$\mathbb{VAR}[P] = \frac{\alpha(C_{k,l}\rho_p)^2 K}{(\pi\lambda_{pt})^{\alpha-1}(\alpha-1)}\left(\Gamma(\alpha+1) - \left(\Gamma\left(\frac{\alpha}{2}+1\right)\right)^2(1-K)\right). \tag{7}$$

Via moment matching, shape and scale parameters k_P and θ_P are obtained as $k_P = \frac{(\mathbb{E}[P])^2}{\mathbb{VAR}[P]}$ and $\theta_P = \frac{\mathbb{VAR}[P]}{\mathbb{E}[P]}$.

A. Derivation of $C_{k,l}$

All K sub-bands used by the primary transmitter $\phi_{pt,l}$ have equal probabilities to be assigned for communication with a primary receiver, and thus $C_{k,l}$ remains constant $\forall k \in \{1, 2, ..., K\}$. From intuition, $C_{k,l}$ depends on the number of primary receivers associated with $\phi_{pt,l}$, which is

itself dependent on the area of its Voronoii cell. However, the area of a Voronoii cell has no exact distribution. But, an accurate approximation can be made using the Gamma distribution [46]. If $\mathcal{B}$ and $\bar{\mathcal{B}}$ are the cell area and average cell area, the normalized area $\tilde{\mathcal{B}} = \frac{\mathcal{B}}{\bar{\mathcal{B}}}$ of a Voronoii cell is given by $f_{\tilde{\mathcal{B}}}(x) = \frac{\beta_v^{\mu_v}}{\Gamma(\mu_v)} x^{\mu_v - 1} e^{-\beta_v x}$, where $\beta_v = 3.57$, $\mu_v = 3.61$, and $\bar{\mathcal{B}} = \frac{1}{\lambda_{pt}}$.

If the number of primary receivers associated with $\phi_{pt,l}$ is Z, $C_{k,l}$ can be expressed as

$$C_{k,l} \backslash z = \Pr[Z \geq K] + \sum_{z=1}^{K-1} \Pr[Z = z] \frac{z}{K}. \tag{8}$$

Using (1) for a given area $\mathcal{B}$ and subsequent averaging by the distribution of $f_{\tilde{\mathcal{B}}}(x)$ results in

$$C_{k,l} = \frac{\beta_v^{\mu_v}}{\Gamma(\mu_v)} \left(\sum_{z=K}^{\infty} \frac{\Gamma(\mu_v + z) \eta^z}{z! (\beta_v + \eta)^{\mu_v + z}} + \sum_{z=1}^{K-1} \frac{\Gamma(\mu_v + z) \eta^z}{K (z-1)! (\beta_v + \eta)^{\mu_v + z}} \right), \tag{9}$$

where $\eta = \frac{\lambda_{pr}}{\lambda_{pt}}$.

IV. D2D Transmission Probability

In this section, we derive the transmission probability of a D2D transmitter for the four energy harvesting schemes. For all four schemes, we assume that the energy level drops to 0 after a transmission. Moreover, we assume that each D2D transmitter has data to be transmitted at the start of a given time slot.

A. Single slot harvest

This scheme is described in Page 11, where node $\mathcal{D}_t$ attempts a transmission irrespective of the energy harvest provided $\mathcal{D}_t$ lies outside the guard region. The distance between the node $\mathcal{D}_t \in \Phi_{d2d}$ and its receiver, r_{d2d}, is distributed as (3). If the harvested energy $\beta PT > \rho_{d2d} r_{d2d}^{\alpha} T$, the transmitted power $P_{\mathcal{D}_t} = \rho_{d2d} r_{d2d}^{\alpha}$. However, whenever $\beta PT < \rho_{d2d} r_{d2d}^{\alpha} T$, $P_{\mathcal{D}_t} = \beta P$. Therefore, $\tau = \Pr[P_{\mathcal{D}_t} = \beta P]$ can be obtained as

$$\begin{aligned} \tau &= \Pr\left[P < \frac{\rho_{d2d} r_{d2d}^{\alpha}}{\beta} \right] \\ &= \int_0^{d_l} \frac{2x}{d_l^2 \Gamma(k_P)} \gamma\left(k_P, \frac{\rho_{d2d} x^{\alpha}}{\beta \theta_P} \right) dx, \end{aligned} \tag{10}$$

where (10) is obtained after first evaluating τ conditioned on r_{d2d}, and then averaging over (3).

Let p^{ss} be the probability that $\mathcal{D}_t$ is ready to transmit at the start of a time slot at steady state. Due to the temporal effects, we use a two state Markov chain: charged (state 1) and uncharged (state 0). While $\mathcal{D}_t$ always transitions from the uncharged state to the charged state at the start

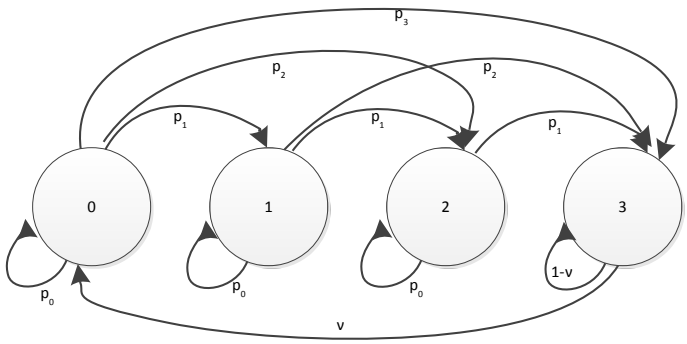

Fig. 2: Markov chain model for multi-slot harvesting with $M = 3$.

of the next time slot, it only transitions from the charged state to the uncharged state if it lies outside the guard region $\mathcal{A}_{\mathcal{G}}$. The state transition matrix Q can be written as

$$Q = \begin{bmatrix} 0 & 1 \\ \nu & 1-\nu \end{bmatrix}.$$

Let $\Omega = [\omega_0 \ \omega_1]$ be the vector comprising steady state probabilities of Q. During steady state, $\Omega = \Omega Q$, and we can derive $p^{ss} = \omega_1 = \frac{1}{1+\nu}$. Thus, the probability of conducting a transmission at the start of a time slot is νp^{ss}.

B. Multi-slot harvest

As mentioned in Section II, under multi-slot harvesting, node $\mathcal{D}_t$ harvests energy in multiple time slots until the total harvested energy βPT is greater than the maximum energy required to transmit, which is $\rho_{d2d} d_l^{\alpha} T$. While the harvested energy at the end of a time slot does not confine to discrete levels, for mathematical convenience, we divide the energy levels into $M+1$ discrete states where M can be increased arbitrarily to better reflect the non-discrete nature of the energy level. The 0-th and M-th states respectively denotes the uncharged and fully charged levels. Let the power level of the δ-th state ($0 < \delta < M$) be denoted as E_δ. If $\mathcal{D}_t$ was initially in state 0, it would transition to state δ whenever $E_\delta \leq \beta PT < E_{\delta+1}$, remain at state 0 if $\beta PT < E_1$, and reach state M if $\beta PT \geq E_M$. Similarly, whenever $\mathcal{D}_t$ is initially at state δ, the transitioned state increases correspondingly.

The state transition diagram is in Fig. 2, and the state transition matrix Q (with the vector of steady state probabilities being $\Omega = [\omega_0 \ \omega_1 \ . \ . \ \omega_M]$) is expressed as follows.

$$Q = \begin{bmatrix} p_0 & p_1 & p_2 & . & p_{M-1} & 1-\sum_{g=0}^{M-1} p_g \\ 0 & p_0 & p_1 & . & p_{M-2} & 1-\sum_{g=0}^{M-2} p_g \\ 0 & 0 & p_0 & . & p_{M-3} & 1-\sum_{g=0}^{M-3} p_g \\ . & . & . & . & . & . \\ 0 & 0 & 0 & . & p_0 & 1-p_0 \\ \nu & 0 & 0 & . & 0 & 1-\nu \end{bmatrix}.$$

Here $p_g (g \in \{1, 2, 3, ..., M-1\})$ refers to the probability of transitioning g states higher from the initial state, and can be expressed as

$$\begin{aligned} p_g &= \Pr\left[\frac{g\rho_{d2d} d_l^{\alpha}}{\beta M} \leq P < \frac{(g+1)\rho_{d2d} d_l^{\alpha}}{\beta M}\right] \\ &= \frac{1}{\Gamma(k_P)}\left(\gamma\left(k_P, \frac{(g+1)\rho_{d2d} d_l^{\alpha}}{\beta M \theta_P}\right) - \gamma\left(k_P, \frac{g\rho_{d2d} d_l^{\alpha}}{\beta M \theta_P}\right)\right). \end{aligned} \tag{11}$$

Let p^{ms} be the probability that $\mathcal{D}_t$ is ready to transmit at the start of a time slot, which is also the steady state probability of being at state M. We can obtain p^{ms} as

$$p^{ms} = \omega_M = \frac{1}{1 + \sum_{g=0}^{M-1} \mathcal{D}_g}. \tag{12}$$

Here, $\mathcal{D}_0 = \frac{-\nu}{p_0 - 1}$, and $\mathcal{D}_g = \frac{-1}{p_0 - 1}(\sum_{h=0}^{g-1} p_{g-h}\mathcal{D}_h)$ for $1 \leq g \leq M-1$. It can be easily seen that (12) reduces to p^{ss} when $M = 1$ and $p_0 = 0$. The probability of conducting a transmission at the start of any time slot is thus νp^{ms}.

C. $\mathcal{N}$ slot harvest

Let $\beta P_{T,\mathcal{N}} T$ be the harvested energy at the end of $\mathcal{N}$ time slots. $P_{T,\mathcal{N}}$ is written as

$$P_{T,\mathcal{N}} = P_1 + P_2 + \cdots + P_{\mathcal{N}}, \tag{13}$$

where $P_w, w \in \{1, 2, \ldots, \mathcal{N}\}$ is the ambient power available to be harvested during the w-th time slot. It should be noted that $P_w \ \forall w$ are independent and identically distributed random variables having the distribution of P (Gamma with shape and scale parameters k_P and θ_P). As such, $P_{T,\mathcal{N}}$ is also Gamma distributed with shape and scale parameters $\mathcal{N}k_P$ and θ_P respectively.

Whenever the harvested energy $\beta P_{T,\mathcal{N}} T > \rho_{d2d} r_{d2d}^{\alpha} T$, the transmit power $P_{\mathcal{D}_t} = \rho_{d2d} r_{d2d}^{\alpha}$. But, when $\beta P_{T,\mathcal{N}} T < \rho_{d2d} r_{d2d}^{\alpha} T$, $P_{\mathcal{D}_t} = \beta P_{T,\mathcal{N}}$ because transmission occurs after $\mathcal{N}$ slots irrespective of the harvested energy. Thus, we can write $\tau = \Pr[P_{\mathcal{D}_t} = \beta P_{T,\mathcal{N}}]$ as

$$\begin{aligned}\tau &= \Pr[P_{T,\mathcal{N}} < \frac{\rho_{d2d} r_{d2d}^{\alpha}}{\beta}] \\ &= \int_0^{d_l} \frac{2x}{d_l^2 \Gamma(\mathcal{N} k_P)} \gamma\left(\mathcal{N} k_P, \frac{\rho_{d2d} x^{\alpha}}{\beta \theta_P}\right) dx. \end{aligned} \tag{14}$$

We now require the probability that a typical D2D transmitter $\mathcal{D}_t$ is ready to transmit at the start of a given time slot, which is denoted by $p^{\mathcal{N}s}$. Similar to the previous schemes, we will use a Markov chain in order to account for the temporal effects. This chain will have $\mathcal{N}+1$ states, where the δ-th state ($0 \leq \delta \leq \mathcal{N}$) corresponds to the state after charging for δ time slots. As such, the 0-th state is the uncharged state while the $\mathcal{N}$-th state is the state where transmission is conducted. While the current state $\delta < \mathcal{N}$, transition always occurs to the subsequent state $(\delta+1)$ after charging for a time slot. When the current state is $\mathcal{N}$, transmission can occur whenever $\mathcal{D}_t$ is outside the guard region $\mathcal{A}_{\mathcal{G}}$, and a transition occurs to the 0-th state. Conversely, whenever $\mathcal{D}_t$ is located within $\mathcal{A}_{\mathcal{G}}$, no transmission occurs and the state remains at $\mathcal{N}$. This can be written as a state transition matrix Q where

$$Q = \begin{bmatrix} 0 & 1 & 0 & . & 0 & 0 \\ 0 & 0 & 1 & . & 0 & 0 \\ . & . & . & . & . & . \\ 0 & 0 & 0 & . & 1 & 0 \\ 0 & 0 & 0 & . & 0 & 1 \\ \nu & 0 & 0 & . & 0 & 1-\nu \end{bmatrix}.$$

Let $\Omega = [\omega_0 \ \omega_1 \dots \omega_{\mathcal{N}}]$ be the steady state probability vector. $p^{\mathcal{N}s}$ is thus equivalent to $\omega_{\mathcal{N}}$, which is the steady state probability of being at state $\mathcal{N}$. Thus we can obtain $p^{\mathcal{N}s}$ as

$$p^{\mathcal{N}s} = \frac{1}{1+\mathcal{N}\nu}. \tag{15}$$

It can be observed that $p^{\mathcal{N}s}$ reduces to p^{ss} whenever $\mathcal{N} = 1$. The probability of $\mathcal{D}_t$ conducting a transmission at the start of any time slot is thus $\nu p^{\mathcal{N}s}$.

D. Hybrid harvest

The state transition diagram for this harvesting scheme is shown in Fig. 3. It should be noted that while the states of Fig. 2 represented distinct levels of energy, the states in Fig. 3 represent

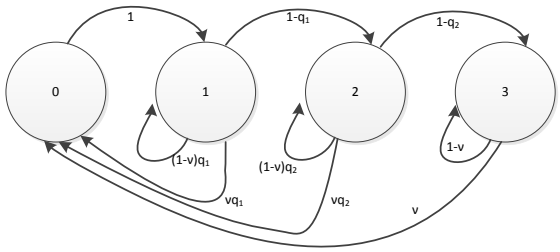

Fig. 3: Markov chain model for hybrid harvesting with $\mathcal{N} = 3$.

the states after particular time slots. Similar to the $\mathcal{N}$ slot harvesting scheme, the Markov chain will have $\mathcal{N}+1$ states. While the δ-th state ($0 \leq \delta \leq \mathcal{N}$) corresponds to the state after charging for δ time slots similar to the $\mathcal{N}$ slot harvesting scheme, there are some notable differences as well. If the D2D transmitter is fully charged at the δ-th state, it either remains within that state if it's within the guard region $\mathcal{A}_{\mathcal{G}}$ or transmits and transitions back to the 0-th uncharged state if outside $\mathcal{A}_{\mathcal{G}}$.

Let the harvested energy after w time slots ($0 < w \leq \mathcal{N}$) be $\beta P_{T,w} T$. As described in the previous subsection (Section III C), $P_{T,w}$ follows a Gamma distribution with shape and scale parameters of wk_P and θ_P. If q_w is the probability that the D2D transmitter harvests sufficient energy after w time slots, q_w can be expressed as follows.

$$\begin{aligned} q_w &= \Pr\left[\beta P_{T,w} T > \rho_{d2d} r_{d2d}^{\alpha} T\right] \\ &= 1 - \int_0^{d_l} \frac{2x}{d_l^2 \Gamma(wk_P)} \gamma\left(wk_P, \frac{\rho_{d2d} x^{\alpha}}{\beta \theta_P}\right) dx. \end{aligned} \tag{16}$$

Now, we will evaluate the probability that the transmit power of node $\mathcal{D}_t$ $P_{\mathcal{D}_t} \neq \rho_{d2d} r_{d2d}^{\alpha}$. After $\mathcal{N}$ time slots, transmission occurs irrespective of the harvested energy. Therefore, if $\mathcal{D}_t$ harvests energy for the full $\mathcal{N}$ time slots, and if the harvested energy $\beta P_{T,\mathcal{N}} T < \rho_{d2d} r_{d2d}^{\alpha} T$, $P_{\mathcal{D}_t} = \beta P_{T,\mathcal{N}}$. Thus, we can express $\tau = \Pr[P_{\mathcal{D}_t} = \beta P_{T,\mathcal{N}}]$ as

$$\tau = \prod_{w=1}^{\mathcal{N}} (1 - q_w), \tag{17}$$

where q_w is given in (16).

$$\omega_0 = \frac{1}{1 + \frac{1}{(1-(1-\nu)q_1)} + \sum_{\delta=2}^{\mathcal{N}-1} \frac{\prod_{g=1}^{\delta-1}(1-q_g)}{\prod_{h=1}^{\delta}(1-(1-\nu)q_h)} + \frac{\prod_{g=1}^{\mathcal{N}-1}(1-q_g)}{\nu \prod_{h=1}^{\mathcal{N}-1}(1-(1-\nu)q_h)}} \tag{19}$$

The state transition matrix Q is written as

$$Q = \begin{bmatrix} 0 & 1 & 0 & . & 0 & 0 \\ \nu q_1 & (1-\nu)q_1 & 1-q_1 & . & 0 & 0 \\ . & . & . & . & . & . \\ \nu q_{\mathcal{N}-2} & 0 & 0 & . & q_{\mathcal{N}-1} & 0 \\ \nu q_{\mathcal{N}-1} & 0 & 0 & . & (1-\nu)q_{\mathcal{N}-1} & 1-q_{\mathcal{N}-1} \\ \nu & 0 & 0 & . & 0 & 1-\nu \end{bmatrix}.$$

Let $\Omega = [\omega_0\ \omega_1 \dots \omega_{\mathcal{N}}]$ be the steady state probability vector. During steady state, $\Omega = \Omega Q$. After solving this expression for different $\omega_\delta (\delta \in \{0, 1, \dots, \mathcal{N}\})$, we obtain

$$\omega_\delta = \begin{cases} \frac{1}{(1-(1-\nu)q_1)}\omega_0 \ , \ \delta = 1 \\ \frac{\prod_{g=1}^{\delta-1}(1-q_g)}{\prod_{h=1}^{\delta}(1-(1-\nu)q_h)}\omega_0 \ , \ \delta = 2, 3, \dots, \mathcal{N}-1 \\ \frac{\prod_{g=1}^{\delta-1}(1-q_g)}{\nu \prod_{h=1}^{\delta-1}(1-(1-\nu)q_h)}\omega_0 \ , \ \delta = \mathcal{N} \end{cases}, \tag{18}$$

where ω_0 is given in (19).

Let p^{hs} be the probability that $\mathcal{D}_t$ is ready to transmit at the beginning of a particular time slot under the hybrid harvesting scheme. This probability is composed of multiple components where each component comprises the ready-to-transmit probability after each harvesting slot. Thus, we may write p^{hs} as

$$p^{hs} = \sum_{\delta=1}^{\mathcal{N}-1} \omega_\delta q_\delta + \omega_{\mathcal{N}}, \mathcal{N} \geq 2. \tag{20}$$

Whenever $\mathcal{N} = 1$, the hybrid harvesting scheme reduces to the single slot harvesting scheme. The probability of the D2D transmitter $\mathcal{D}_t$ actually conducting a transmission is therefore written as νp^{hs}.

V. D2D Receiver Performance

Here we analyze the coverage performance of a D2D receiver where each D2D transmitter randomly selects a sub-band $k (k \in \{1, 2, ..., K\})$ when it is ready to transmit. If γ_{d2d} is the SINR at the D2D receiver associated with $\mathcal{D}_t$, we can write it as $\gamma_{d2d} = \frac{P_{d2d,j}}{I_P + I_{d2d} + \sigma_n^2}$, where $P_{d2d,j}$

$$\mathbb{P}_C=\int_{r_{d2d}=0}^{d_l}\int_{P=0}^{\frac{\rho_{d2d}r_{d2d}^{\alpha}}{\beta}} e^{\frac{-\sigma_n^2\gamma_T r_{d2d}^{\alpha}}{\beta P}} M_{I_p}(\frac{\gamma_T r_{d2d}^{\alpha}}{\beta P})\frac{P^{k_P-1}e^{-\frac{P}{\theta_P}}}{\Gamma(k_P)\theta_P}\frac{2r_{d2d}}{d_l^2}dPdr_{d2d}+(1-\tau)e^{\frac{-\sigma_n^2\gamma_T}{\rho_{d2d}}}M_{I_p}(\frac{\gamma_T}{\rho_{d2d}})M_{I_{d2d}}(\frac{\gamma_T}{\rho_{d2d}}) \quad (22)$$

is the received power from $\mathcal{D}_t$, I_P is the interference from primary signals within the k-th sub band, I_{d2d} is the interference from other D2D transmissions, and σ_n^2 is the noise power.

Coverage occurs if $\gamma_{d2d} > \gamma_T$, where γ_T is a threshold SINR level. Coverage probability $\mathbb{P}_C = \Pr[\gamma_{d2d} > \gamma_T]$ may thus be expressed as

$$\begin{aligned}\mathbb{P}_C = \tau \Pr\left[\frac{\beta P|h_{d2d}|r_{d2d}^{-\alpha}}{I_P + I_{d2d} + \sigma_n^2} > \gamma_T\right] \\ + (1-\tau)\Pr\left[\frac{\rho_{d2d}|h_{d2d}|}{I_P + I_{d2d} + \sigma_n^2} > \gamma_T\right],\end{aligned} \quad (21)$$

where τ is defined in (10). Note that for the multi slot harvesting scheme $\tau = 0$, and the first term of (21) vanishes. After several mathematical manipulations and ignoring the negligible interference from D2D transmitters when a full charge does not occur (for the single slot scheme), we can express $\mathbb{P}_C$ as (22) where the remaining integrals must be performed numerically. However, in order to evaluate (22), the MGFs of I_p and I_{d2d} are needed.

The interference from primary network is composed of signals from k-th sub band primary transmitters. Thus, these interfering primary transmitters form a thinned homogeneous Poisson point process with density $C_{k,l}\lambda_{pt}$, where $C_{k,l}$ follows (9), and the interference from a single primary transmitter $\phi_{pt,l}$ is written as $I_{P,l} = \rho_p \hat{r}_{k,l}^{\alpha}|h_{l,r}|^2 g(r_{l,r})$, where $|h_{l,r}|^2$ and $g(r_{l,r}) = r_{l,r}^{-\alpha}$ are respectively the channel power gain and path loss between the l-th interfering primary transmitter and the receiver associated with $\mathcal{D}_t$. Thus, making use of Slyvniak's and Campbell's theorems, we can write $M_{I_p}(s) = e^{\left(\int_0^{\infty}\mathbb{E}\left[e^{-s\rho_p\hat{r}_{k,l}^{\alpha}|h_{l,r}|^2 r_{l,r}^{-\alpha}}-1\right]2\pi C_{k,l}\lambda_{pt}r_{l,r}dr_{l,r}\right)}$. After first averaging with respect to $|h_{l,r}|$, performing the integral, and finally averaging with respect to $\hat{r}_{k,l}$ we get

$$M_{I_p}(s) = e^{\left(-\frac{2\pi^2 C_{k,l}\lambda_{p,t}(s\rho_p)^{\frac{2}{\alpha}}}{\alpha sin\left(\frac{2\pi}{\alpha}\right)}\mathbb{E}[\hat{r}_{k,l}^2]\right)} = e^{\left(-\frac{2\pi C_{k,l}(s\rho_p)^{\frac{2}{\alpha}}}{\alpha sin\left(\frac{2\pi}{\alpha}\right)}\right)}. \quad (23)$$

We now focus our attention on deriving the MGF of I_{d2d}. I_{d2d} is composed of the interference from other D2D transmitters occupying the k-th sub band. For interference to occur from the jj-th D2D transmitter, it must be ready to transmit, be outside guard regions, and must choose the k-th sub band. As these conditions occur independently from other D2D transmitters within Φ_{d2d}, the interfering D2D transmitters can be approximated by a thinned homogeneous Poisson

point process with a density of $\frac{\nu p^* \lambda_{d2d}}{K}$, where $* \in \{ss, ms\}$. Now the interference from the jj-th D2D transmitter can be written as $I_{d2d,jj} = P_{jj}|h_{jj,r}|^2 g(r_{jj,r})$, where $|h_{jj,r}|^2$ and $g(r_{jj,r}) = r_{jj,r}^{-\alpha}$ are the channel power gain and path loss between the jj-th interfering D2D transmitter and the receiver associated with $\mathcal{D}_t$, while P_{jj} is the transmit power of the jj-th interfering D2D transmitter. Using a similar method to the derivation of (23), we can write $M_{I_{d2d}}$ as

$$M_{I_{d2d}} = e^{\left(-\frac{2\pi^2 \nu p^* \lambda_{d2d} s^{\frac{2}{\alpha}}}{\alpha K sin\left(\frac{2\pi}{\alpha}\right)} \mathbb{E}[P_{jj}^{\frac{2}{\alpha}}]\right)}. \tag{24}$$

The expectation $\mathbb{E}[P_{jj}^{\frac{2}{\alpha}}]$ can be expressed as

$$\mathbb{E}[P_{jj}^{\frac{2}{\alpha}}] = \tau \mathbb{E}[\beta^{\frac{2}{\alpha}} P^{\frac{2}{\alpha}}] + (1-\tau)\mathbb{E}[\rho_{d2d}^{\frac{2}{\alpha}} r_{d2d}^2], \tag{25}$$

where the first and second expectations are respectively with respect to P given that $P < \frac{\rho_{d2d} r_{d2d}^{\alpha}}{\beta}$ and r_{d2d}. It should be noted that for the multi slot harvesting scheme $\tau = 0$, and the first term will disappear. Thus, after some mathematical modifications, we obtain

$$\mathbb{E}[P_{jj}^{\frac{2}{\alpha}}] = \int_0^{d_l} \frac{2x(\beta\theta_P)^{\frac{2}{\alpha}}}{\Gamma(k_P) d_l^2} \gamma\left(k_P + \frac{2}{\alpha}, \frac{\rho_{d2d} x^{\alpha}}{\beta\theta_P}\right) dx + (1-\tau)\frac{\rho_{d2d}^{\frac{2}{\alpha}} d_l^2}{2}. \tag{26}$$

1) Probability of a successful transmission: The final probability of a successful transmission during a given time slot ($\mathbb{P}_{C,Total}$) depends on three factors. First, the D2D transmitter should be in the charged state at the start of the time slot. Second, it should not be inside any guard region. Third, if a transmission occurs, the D2D receiver should be within coverage. Considering all three conditions, we can write

$$\mathbb{P}_{C,Total} = p^* \nu \mathbb{P}_C. \tag{27}$$

VI. Numerical Results

Within this section, we investigate the probability of being able to transmit at the start of a particular time slot and the successful transmission probability ($\mathbb{P}_{C,Total}$) of an energy harvesting D2D transmitter. Simulation was conducted in MATLAB, and the parameter values of $K = 10$, $\lambda_{d2d} = 10^{-3}$, $\alpha = 2.5$, $\rho_p = -100\,\text{dBm}$, $d_g = 10$, $M = 5$, $\beta = 0.5$, $\gamma_T = -30\,\text{dB}$ were used unless otherwise mentioned.

First, we plot the probability of each D2D transmitter being able to transmit (p, $p \in \{p^{ss}, p^{ms}, p^{\mathcal{N}s}, p^{hs}\}$) vs. the primary receiver density λ_{pr} for all the energy harvesting schemes in Fig. 4. Because energy is harvested during a single time slot, the single slot harvesting scheme has the highest probability of being able to transmit, and thus p^{ss} is the highest. The $\mathcal{N}$ slot and hybrid harvesting

schemes follow next with the hybrid scheme showing a slightly higher probability which is not easily identifiable within the figure. When λ_{pr} increases, p^{ss}, $p^{\mathcal{N}s}$, and p^{hs} approach 1. Counter-intuitively, this is due to the actual transmission probability (νp) getting lower because of the larger area getting earmarked as guard regions. Thus, the probability that a D2D transmitter gets stuck being able to transmit, but without being allowed to transmit is higher. From the figure, it is evident that the the multi slot harvesting scheme fares the worst in terms of p. However, as we will see in the subsequent plots, it will have better total coverage under certain conditions. Moreover, as λ_{pr} increases beyond $-40\,\text{dB}$, p^{ms} keeps relatively constant, which is contrary to the other three schemes. The different performance trend of the multi slot scheme is due to it being a scheme based on the harvested energy level as opposed to the number of harvesting slots.

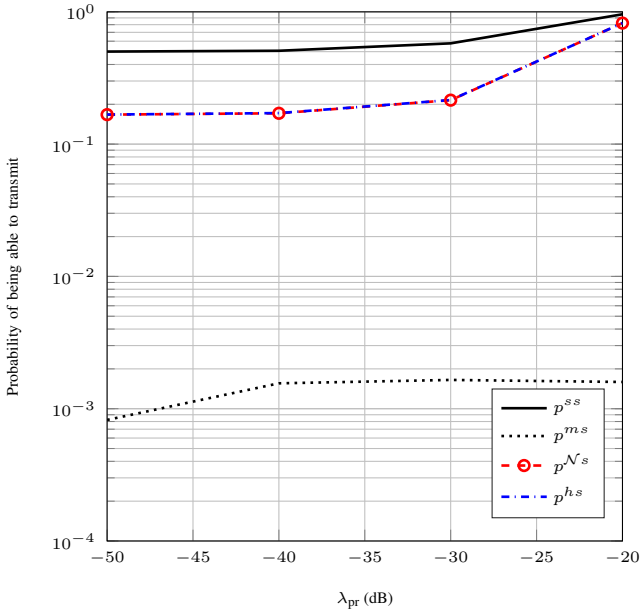

Fig. 4: The probability of being able to transmit ($p^{ss}, p^{ms}, p^{\mathcal{N}s}, p^{hs}$) vs. λ_{pr} for the different energy harvesting schemes. $\rho_{d2d} = -100\,\text{dBm}$, $\mathcal{N} = 5$, $d_l = 100$, and $\lambda_{pt} = 10^{-5}$.

In the subsequent figures, we investigate how different system parameters effect the total coverage probability $\mathbb{P}_{C,Total}$. To this end, we plot $\mathbb{P}_{C,Total}$ vs. the threshold SINR level γ_T in Fig. 5. Except when $\gamma_T = -50\,\text{dB}$, single slot harvesting has the lowest total coverage. Increasing the number of harvesting time slots ($\mathcal{N}$) to 5 with $\mathcal{N}$ slot harvesting significantly increases the performance. Moreover, the performance increases further when hybrid harvesting is employed for $\mathcal{N} = 5$. Furthermore, while the rate of coverage drop as γ_T increases is similar for the

single slot and $\mathcal{N}$ slot harvesting, hybrid harvesting has a lower rate of decrease. The multi slot harvesting scheme shows a different trend compared to the other three schemes. While it has the worst performance for very low γ_T, its relative performance compared to the other schemes increases as γ_T is increased. For high γ_T, the total coverage is mostly affected by the transmitted signal falling below the SINR threshold. Because multi-slot harvesting ensures a high harvest, the resultant transmission is more likely to be successful. However, the other schemes do not ensure a sufficient harvest, and thus are adversely effected when γ_T increases.

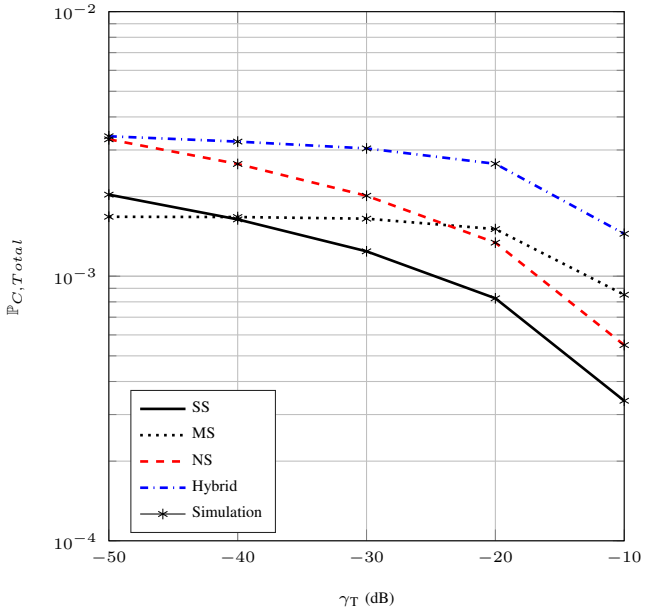

Fig. 5: $\mathbb{P}_{C,Total}$ vs. γ_T for the different energy harvesting schemes. $\rho_{d2d} = -100$ dBm, $d_l = 100$, $\lambda_{pr} = 10^{-3}$, $\mathcal{N} = 5$ and $\lambda_{pt} = 10^{-5}$.

In Fig. 6, we plot the total coverage probability $\mathbb{P}_{C,Total}$ with respect to the path loss exponent α. $\mathbb{P}_{C,Total}$ drops as α increases for all harvesting schemes. However, the rate of decrease reduces with α as well. $\mathcal{N}$ slot harvesting with $\mathcal{N} = 5$ has a significant better coverage than single slot harvesting, and hybrid harvesting with $\mathcal{N} = 5$ has even better coverage performance. While $\mathcal{N}$ slot has a lower probability of being able to transmit compared to single slot harvesting, the resulting transmissions are more successful due to more energy being harvested. Moreover, hybrid harvesting improves on $\mathcal{N}$ slot harvesting by having a higher probability of being able to transmit. Similar to previous figures, multi slot harvesting shows a different trend; the rate of coverage decrease is lower compared to other schemes. Thus, for very high path loss exponents, multi slot harvesting has the best coverage performance.

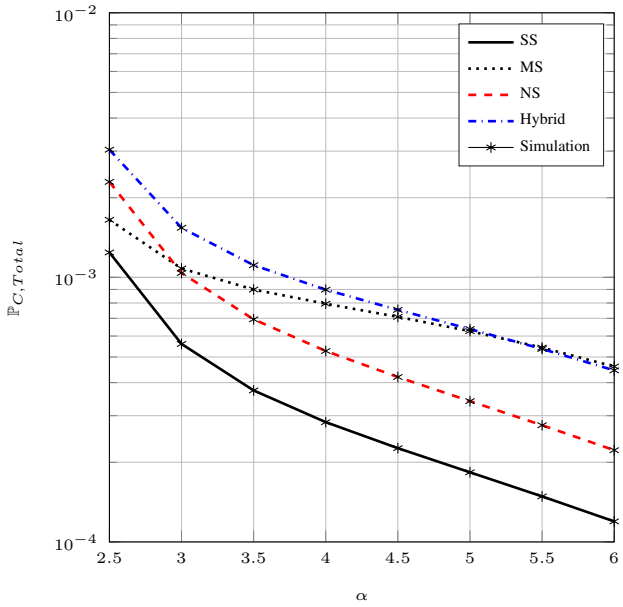

Fig. 6: $\mathbb{P}_{C,Total}$ vs. α for the different energy harvesting schemes. $\rho_{d2d} = -100\,\text{dBm}$, $d_l = 100$, $\lambda_{pr} = 10^{-3}$, $\mathcal{N} = 5$ and $\lambda_{pt} = 10^{-5}$.

Fig. 7 plots $\mathbb{P}_{C,Total}$ vs. the D2D receiver sensitivity ρ_{d2d} for the single slot and multi slot harvesting schemes. While $\mathbb{P}_{C,Total}$ increases and keeps constant with ρ_{d2d} for single slot harvesting, the trend is drastically different for multi slot harvesting where $\mathbb{P}_{C,Total}$ drops sharply. For single slot harvesting, increasing ρ_{d2d} is counter productive because the probability of acquiring the increased energy is low. However, for multi slot harvesting, increasing ρ_{d2d} significantly reduces p^{ms} as this scheme always ensures that the required power is harvested before a transmission. Moreover, it is interesting to note that while reducing the primary receiver density increases $\mathbb{P}_{C,Total}$ for single slot harvesting, the trend is different for multi slot harvesting. While reducing λ_{pr} increases $\mathbb{P}_{C,Total}$ for low ρ_{d2d}, the opposite is true for high ρ_{d2d}.

$\mathbb{P}_{C,Total}$ is plotted against the D2D transmitter-receiver distance d_l in Fig. 8 for the single slot and multi slot harvesting schemes. While increasing d_l reduces $\mathbb{P}_{C,Total}$ as expected, the rate of decrease varies significantly for different primary transmitter densities and the energy harvesting scheme. When $\lambda_{pt} = 1\times10^{-5}$, the multi slot harvesting scheme always outperforms the single slot scheme, and the successful transmission probability is consistently low. When $\lambda_{pt} = 1 \times 10^{-4}$, the coverage performance increases, for both energy harvesting schemes. However, while the multi slot scheme performs better when d_l is lower, the opposite is true for higher d_l. When λ_{pt} is increased further to 1×10^{-5}, the single slot scheme performs better under all d_l values.

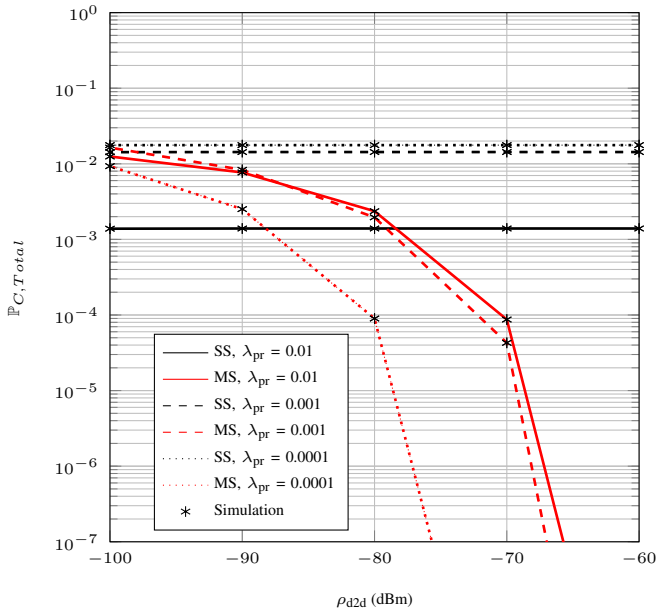

Fig. 7: $\mathbb{P}_{C,Total}$ vs. ρ_{d2d} for SS and MS energy harvesting. $d_l = 100$, $\lambda_{pr} = 10^{-3}$, and $\lambda_{pt} = 10^{-4}$.

Moreover, the performance of the multi slot energy harvesting drops drastically as d_l increases. With a higher d_l, a higher power is required for transmission, and with the MS scheme, the D2D transmitter must wait till fully charged before it can transmit. However, because λ_{pt} is high, the powers of the primary transmitters are low due to lower transmitter receiver distances, which means smaller amounts of energy available for harvesting during each time slot. As such, p^{ms} drops significantly, and thus $\mathbb{P}_{C,Total}$ as well.

We now investigate the effects of different $\mathcal{N}$ on $\mathcal{N}$ slot and hybrid harvesting schemes. To this end, we plot $\mathbb{P}_{C,Total}$ vs. ρ_p in Fig. 9. For the corresponding $\mathcal{N}$ value, hybrid harvesting always has better coverage than $\mathcal{N}$ slot harvesting. Moreover, as $\mathcal{N}$ increases, the coverage increases for both schemes. As ρ_p increases, all curves are relatively flat or show a slight increase in coverage till approximately -80 dBm. However, after this value, the coverage drops steadily. When ρ_p increases two affects occur which have contrasting effects on the coverage. First, as the transmit energy of primary transmitters increase to ensure primary receiver sensitivities are met, there is more power to be harvested. Second, the increased primary transmit power causes interference to the D2D transmissions. While the two effects roughly cancel each other out initially, the second effect takes precedence as ρ_p increases. After enough power is harvested to ensure that D2D receiver sensitivities are met, having additional ambient power is not useful for the D2D network because power controlling takes place.

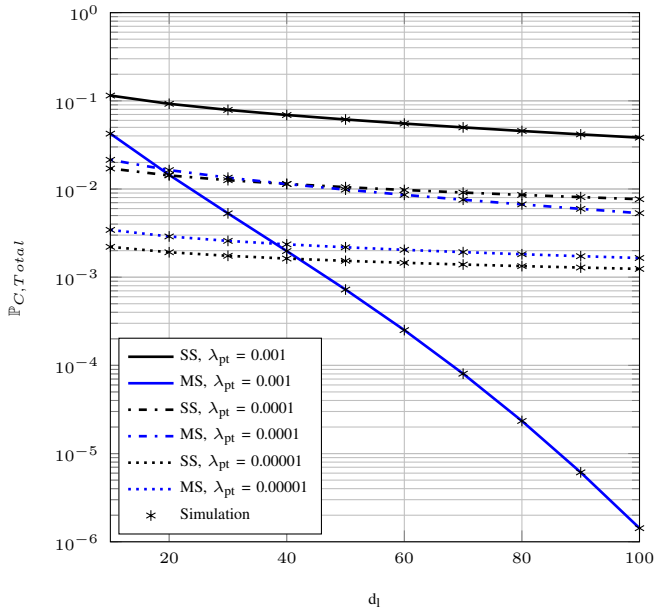

Fig. 8: $\mathbb{P}_{C,Total}$ vs. d_l for SS and MS harvesting. $\rho_{d2d} = -100\,\text{dBm}$, and $\lambda_{pr} = 10^{-3}$.

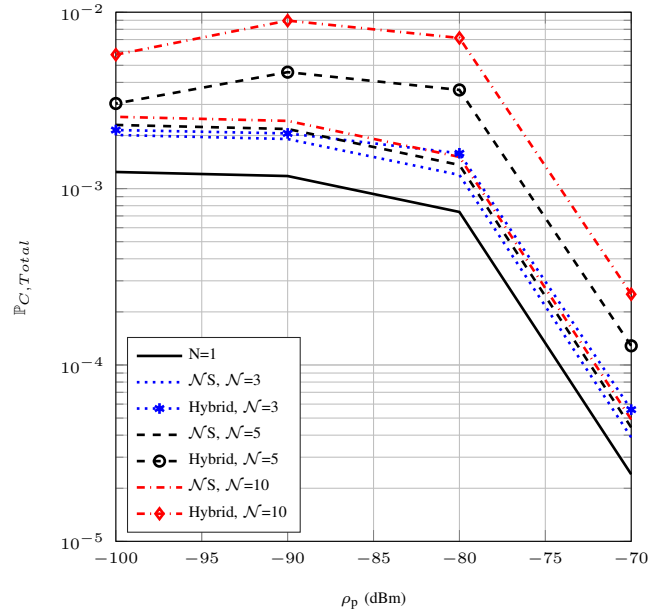

Fig. 9: $\mathbb{P}_{C,Total}$ vs. ρ_p for the $\mathcal{N}$ slot and hybrid harvesting schemes. $\rho_{d2d} = -100\,\text{dBm}$, $d_l = 100$, $\lambda_{pr} = 10^{-3}$, and $\lambda_{pt} = 10^{-5}$.

VII. Conclusion

This paper analyzed the performance of random energy harvesting D2D networks. It considered four energy harvesting schemes and a channel selection protocol where each D2D transmitter selects a primary sub-band randomly. Random fields of primary transmitters and receivers along-

side D2D transmitter-receiver pairs distributed as independent stationary homogeneous Poisson point processes were considered. Multiple sub-channels for primary transmitter-receiver communication, log-distance path loss and Rayleigh fading were assumed. The MGF and other statistics of the ambient RF power at a D2D transmitter were derived and subsequently approximated by a Gamma distribution. Single slot, multi slot, $\mathcal{N}$ slot, and hybrid energy harvesting schemes were proposed, and the probability of successful transmissions were derived for each using a Markov chain based approach incorporating temporal correlations. Moreover, the coverage performance of a D2D link was characterized. Overall, the hybrid harvesting scheme has the best performance among the four proposed schemes. Compared to the other schemes, the multi slot harvesting scheme has different performance trends. It performs better for lower D2D receiver sensitivities, higher SINR thresholds, and higher path loss exponents. Furthermore, the primary transmitter and receiver densities along with reception thresholds significantly affect the total coverage probability of energy harvesting D2D nodes.

REFERENCES

[1] S. Kusaladharma and C. Tellambura, "Performance characterization of spatially random energy harvesting underlay d2d networks with primary user power control," in *Proc. IEEE ICC*, May 2017, pp. 1–6.

[2] Y. Liu, L. Wang, S. A. R. Zaidi, M. Elkashlan, and T. Q. Duong, "Secure D2D communication in large-scale cognitive cellular networks: A wireless power transfer model," *IEEE Trans. Commun.*, vol. 64, no. 1, pp. 329–342, Jan 2016.

[3] S. Kusaladharma and C. Tellambura, "Secondary user interference characterization for spatially random underlay networks with massive mimo and power control," *IEEE Trans. Veh. Technol.*, vol. PP, no. 99, 2017.

[4] A. Sakr and E. Hossain, "Cognitive and energy harvesting-based D2D communication in cellular networks: Stochastic geometry modeling and analysis," *IEEE Trans. Commun.*, vol. 63, no. 5, pp. 1867–1880, May 2015.

[5] Y. Liu, Y. Zhang, R. Yu, and S. Xie, "Integrated energy and spectrum harvesting for 5G wireless communications," *IEEE Netw.*, vol. 29, no. 3, pp. 75–81, May 2015.

[6] S. Atapattu, C. Tellambura, and H. Jiang, *Energy Detection for Spectrum Sensing in Cognitive Radio*. Springer, 2014.

[7] D. Feng, L. Lu, Y. Yuan-Wu, G. Y. Li, S. Li, and G. Feng, "Device-to-device communications in cellular networks," *IEEE Commun. Mag.*, vol. 52, no. 4, pp. 49–55, April 2014.

[8] R. Atat, L. Liu, N. Mastronarde, and Y. Yi, "Energy harvesting-based D2D-assisted machine-type communications," *IEEE Trans. Commun.*, vol. PP, no. 99, pp. 1–1, 2016.

[9] S. Atapattu and J. Evans, "Optimal energy harvesting protocols for wireless relay networks," *IEEE Trans. Wireless Commun.*, vol. 15, no. 8, pp. 5789–5803, Aug 2016.

[10] L. Jiang, H. Tian, Z. Xing, K. Wang, K. Zhang, S. Maharjan, S. Gjessing, and Y. Zhang, "Social-aware energy harvesting device-to-device communications in 5G networks," *IEEE Wireless Commun.*, vol. 23, no. 4, pp. 20–27, August 2016.

[11] G. P. Wijesiri, S. S. Chowdhury, and F. Y. Li, "Energy harvesting-aware backoff algorithms for distributed device-to-device communication," in *Proc. IEEE VTC*, May 2016, pp. 1–5.

[12] Z. Zhou, G. Ma, C. Xu, and Z. Chang, "A game-theoretical approach for green power allocation in energy-harvesting device-to-device communications," in *Proc. IEEE VTC*, May 2016, pp. 1–5.

[13] S. J. Darak, H. Zhang, J. Palicot, and C. Moy, "An efficient policy for D2D communications and energy harvesting in cognitive radios: Go bayesian!" in *Proc. EUSIPCO*, Aug 2015, pp. 1231–1235.

[14] U. Saleem, H. K. Qureshi, S. Jangsher, and M. Saleem, "Transmission power management for throughput maximization in harvesting enabled D2D network," in *Proc. IEEE ISCC*, June 2016, pp. 1078–1083.

[15] T. C. Hsu, Y. W. P. Hong, and T. Y. Wang, "Optimized random deployment of energy harvesting sensors for field reconstruction in analog and digital forwarding systems," *IEEE Trans. Signal Process.*, vol. 63, no. 19, pp. 5194–5209, Oct 2015.

[16] S. Jangsher, H. Zhou, V. O. K. Li, and K. C. Leung, "Joint allocation of resource blocks, power, and energy-harvesting relays in cellular networks," *IEEE J. Sel. Areas Commun.*, vol. 33, no. 3, pp. 482–495, March 2015.

[17] H. H. Yang, J. Lee, and T. Q. S. Quek, "Heterogeneous cellular network with energy harvesting-based D2D communication," *IEEE Trans. Wireless Commun.*, vol. 15, no. 2, pp. 1406–1419, Feb 2016.

[18] S. Lee, R. Zhang, and K. Huang, "Opportunistic wireless energy harvesting in cognitive radio networks," *IEEE Trans. Wireless Commun.*, vol. 12, no. 9, pp. 4788–4799, September 2013.

[19] H. S. Dhillon, Y. Li, P. Nuggehalli, Z. Pi, and J. G. Andrews, "Fundamentals of heterogeneous cellular networks with energy harvesting," *IEEE Trans. Wireless Commun.*, vol. 13, no. 5, pp. 2782–2797, May 2014.

[20] P. Lakhlan and A. Trivedi, "Energy harvesting-based two-hop D2D communication in cellular networks," in *Proc. IEEE ICACCI*, Sept 2016, pp. 328–332.

[21] M. Xie, X. Jia, M. Zhou, and L. Yang, "Study on energy efficiency of D2D underlay massive MIMO networks with power beacons," in *Proc. IEEE WCSP*, Oct 2016, pp. 1–5.

[22] K. Huang, M. Kountouris, and V. O. K. Li, "Renewable powered cellular networks: Energy field modeling and network coverage," *IEEE Transactions on Wireless Communications*, vol. 14, no. 8, pp. 4234–4247, Aug 2015.

[23] S. Gupta, R. Zhang, and L. Hanzo, "Energy harvesting aided device-to-device communication underlaying the cellular downlink," *IEEE Access*, vol. PP, no. 99, pp. 1–1, 2016.

[24] J. Ding, L. Jiang, and C. He, "Dynamic spectrum allocation for energy harvesting-based underlaying D2D communication," in *Proc. IEEE VTC*, May 2016, pp. 1–5.

[25] M. D. Renzo and W. Lu, "System-level analysis and optimization of cellular networks with simultaneous wireless information and power transfer: Stochastic geometry modeling," *IEEE Trans. Veh. Technol.*, vol. 66, no. 3, pp. 2251–2275, March 2017.

[26] P. Guan and M. D. Renzo, "Stochastic geometry analysis and optimization of uplink cellular networks with fractional power control and optimum combining," in *Proc. IEEE ICC*, May 2016, pp. 1–6.

[27] Z. Chen, C.-X. Wang, X. Hong, J. Thompson, S. Vorobyov, X. Ge, H. Xiao, and F. Zhao, "Aggregate interference modeling in cognitive radio networks with power and contention control," *IEEE Trans. Commun.*, vol. 60, no. 2, pp. 456–468, Feb. 2012.

[28] S. Kusaladharma and C. Tellambura, "On approximating the cognitive radio aggregate interference," *IEEE Wireless Commun. Lett.*, vol. 2, no. 1, pp. 58–61, 2013.

[29] H. Dhillon, R. Ganti, F. Baccelli, and J. Andrews, "Modeling and analysis of k-tier downlink heterogeneous cellular networks," *IEEE J. Sel. Areas Commun.*, vol. 30, no. 3, pp. 550–560, April 2012.

[30] J. F. Kingman, *Poisson Processes*. Oxford University Press, 1993.

[31] M. D. Renzo and P. Guan, "Stochastic geometry modeling and system-level analysis of uplink heterogeneous cellular networks with multi-antenna base stations," *IEEE Trans. Commun.*, vol. 64, no. 6, pp. 2453–2476, June 2016.

[32] S. Kusaladharma and C. Tellambura, "Massive MIMO based underlay networks with power control," in *Proc. IEEE ICC*, May 2016, pp. 1–6.

[33] H. ElSawy and E. Hossain, "Two-tier hetnets with cognitive femtocells: Downlink performance modeling and analysis in a multichannel environment," *IEEE Trans. Mobile Comput.*, vol. 13, no. 3, pp. 649–663, March 2014.

[34] A. Goldsmith, *Wireless Communications*. Cambridge University Press, 2005.

[35] A. Molisch, *Wireless Communications*. Wiley-IEEE Press, 2011.

[36] S. Kusaladharma, P. Herath, and C. Tellambura, "Underlay interference analysis of power control and receiver association schemes," *IEEE Trans. Veh. Technol.*, vol. 65, no. 11, pp. 8978–8991, Nov 2016.

[37] S. Kusaladharma, P. Herath, and C. Tellambura, "Impact of transmit power control on aggregate interference in underlay cognitive radio networks," in *Proc. IEEE ICC*, June 2014, pp. 1–6.

[38] T. Bhandari, H. S. Dhillon, and R. M. Buehrer, "The impact of proximate base station measurements on localizability in cellular systems," in *Proc. IEEE SPAWC*, July 2016, pp. 1–5.

[39] C.-H. Lee and C.-Y. Shih, "Coverage analysis of cognitive femtocell networks," *IEEE Wireless Commun. Lett.*, vol. 3, no. 2, pp. 177–180, April 2014.

[40] L. Vijayandran, P. Dharmawansa, T. Ekman, and C. Tellambura, "Analysis of aggregate interference and primary system performance in finite area cognitive radio networks," *IEEE Trans. Commun.*, vol. PP, no. 99, pp. 1–12, 2012.

[41] S. Kusaladharma and C. Tellambura, "Aggregate interference analysis for underlay cognitive radio networks," *IEEE Wireless Commun. Lett.*, vol. 1, no. 6, pp. 641–644, 2012.

[42] C. Tellambura, A. J. Mueller, and V. K. Bhargawa, "Analysis of M-ary phase-shift keying with diversity reception for land-mobile satellite channels," *IEEE Transactions on Vehicular Technology*, vol. 46, no. 4, pp. 910–922, Nov 1997.

[43] C. Tellambura, A. Annamalai, and V. K. Bhargava, "Closed form and infinite series solutions for the MGF of a dual-diversity selection combiner output in bivariate Nakagami fading," *IEEE Transactions on Communications*, vol. 51, no. 4, pp. 539–542, April 2003.

[44] C. Tellambura, "Evaluation of the exact union bound for trellis-coded modulations over fading channels," *IEEE Transactions on Communications*, vol. 44, no. 12, pp. 1693–1699, Dec 1996.

[45] S. Kusaladharma, P. Herath, and C. Tellambura, "Secondary user interference characterization for underlay networks," in *Proc. IEEE VTC*, Sept 2015, pp. 1–5.

[46] J. Ferenc and Z. Neda, "On the size distribution of poisson voronoi cells," *Phisica A: Statistical Mechanics and its Applications*, vol. 385, no. 2, pp. 518–526, Nov 2007.